Plate Motion and Seismic Strain Rate of Western North America

Bryan Beh
Date: 12 December 2018

A report submitted in partial fulfillment of the requirements for the degree of Geophysics at Imperial College London and Associateship of the Royal School of Mines. It is substantially the result of my own work except where explicitly indicated in the text. The report may be freely copied and distributed provided the source is explicitly acknowledged.

Abstract

The Kostrov Summation is used to calculate plate velocity and principal-axes strain rates for areas of earthquake seismicity throughout the western coast of North America. An average percentage difference of 70% was achieved for all calculated values to their corresponding UNAVCO geodetic values. The California region and Gorda region are better represented with calculated results compared to the Explorer region, which may be due largely to complexity of its tectonic regime. Slow earthquakes and aseismic slip contribute to a significant amount of uncertainty within the California and Explorer region. The 42 year period of the CMT Catalogue used also contributes to a large portion of the uncertainty due to absence of important historical earthquakes such as the 1906 San Franciso earthquake. The b-value analysis suggest notable amount of deficit and excess of earthquakes that helped quantify catalogue incompleteness. Variable analysis suggest that all variables except seismogenic thickness was irrelevant in uncertainty analysis. Depth-correction significantly improved accuracy up to 0.4% percentage difference. The study concludes that short term seismicity can represent long term deformation to a sensible accuracy, provided a better constraint of the uncertainties addressed.

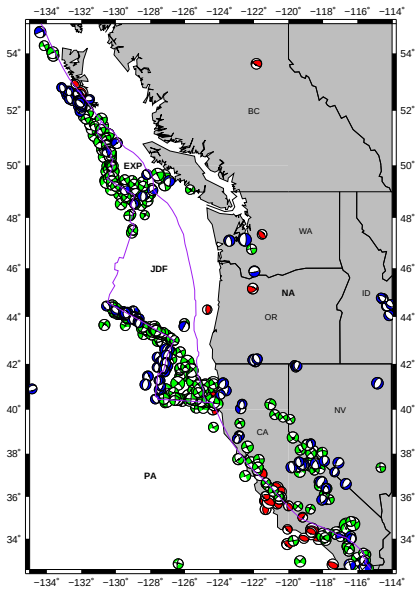

Figure 1. Seismic moment tensor map of Western North America where the purple line is the plate boundary and the beach balls are the focal mechanisms of the earthquake denoted by color. Green represents strike-slip faults, blue represents normal faults and red represents thrust faults. PA, JDF and NA are plate systems Pacific plate, Juan De Fuca Plate and North American Plate respectively.

1. Introduction

The present plate tectonic regime of Western North America involves the relative motion of three main lithospheric plates; the Pacific, American Plates and the smaller Juan De Fuca plate sandwiched between the two. The Juan De Fuca plate in many literatures have been addressed as three smaller segments of the main body: Explorer plate, Juan De Fuca main plate and Gorda Plate as each plate have shown evidence of independent motion (Hyndman and Weichert, 1981).

From the south, the south-east end of the San Andreas Fault system comprises mainly of the southern end of the San Andreas Fault and the San Jacinto Fault (1). The main San Andreas fault extends northwards towards the bottom end of the Transverse Ranges region near Los Angeles (2) where substantial seismicity is also observed. Continuing northwards is the northern end of the Transverse Ranges region and the southern end of the Central California Coast Ranges(3) where the Garlock fault running south-west inter-

sects the San Andreas fault forming a junction North of the Big Bend. Northwards along the Central California Coast Ranges another region of notable seismicity can be seen around the San Francisco Bay Area (5). No significant seismicity is observed at the Northern region of San Andreas. Intraplate deformation is seen at the Nevada-California state boundary which many papers refer to as the Walker Lane fault system (4,6).

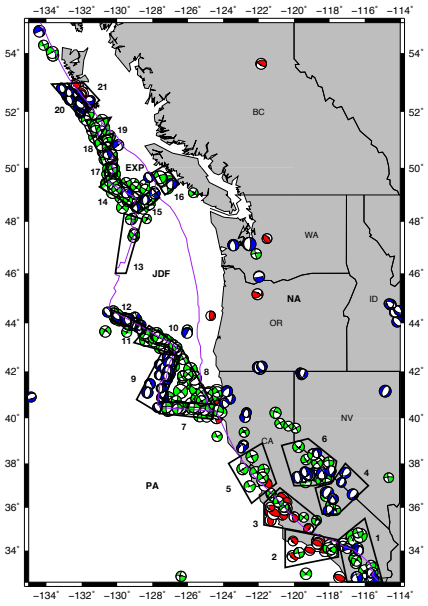

Figure 2. Figure 1 with localised subregions with 1-6 along the San Andreas Fault system, 7-10 along the Gorda plate, 11-14 along the Explorer Plate and 15 along Queen Charlotte Fault.

At the Gorda plate system, the Mendocino fault (7) forms the southern boundary of the Gorda plate and intersects at the Mendocino triple junction with the Cascadia subduction zone and the northern end of the San Andreas fault. This subduction zone remains seismically quiet. A substantial amount of intraplate deformation is also seen within the Gorda plate (8). The westward end of the Mendocino fault connects to the Gorda Ridge (9). The northern end of the Gorda ridge links to the seismically active Blanco fault (10,12) and the Cascadia depression (11), which is connected to the conversely quiet Juan De Fuca ridge.

The northern end of the Juan De Fuca ridge (13) is connected to a triple junction with the Sovanco Fault (14) trending north-westwards and the Nootka Fault (15) trending north-eastwards linking with the Cascadia subduction zone. This triple junction separates the Explorer, Juan De Fuca and Pacific plate. A region of seismicity is also seen sandwiched between the subduction zone and the Vancouver islands (16). The northern end of Sovanco Fault links with the Explorer ridge (17) which is offset by the Revere-Dellwood Fault (18). The Northern end of the Explorer plate contains the Winona Basin (19) south of the Queen Charlotte triple junction. The Queen Charlotte fault (20,21) directly connects the Pacific and American plate. Figure 3 depicts the major faults as described in the study region.

We calculated seismic slip and strain rates of each area (denoted in numbers) through methods that employ earthquake seismic moment tensor data and compare them to published geodetic data. The purpose is to determine whether the long-term deformation of the study region could be represented through short-term seismic deformation of individual earthquakes.

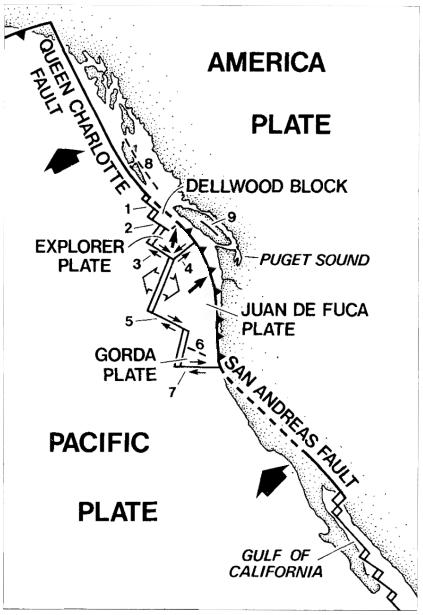

Figure 3. Major faults of Western North America modified from (Hyndman and Weichert, 1981). The numbers 1 - 9 represent the faults: Dellwood-Wilson, Revere-Dellwood, Sovanco, Nootka, Blanco, Gorda, Mendocino, Sandpit and Beaufort. The modified subduction curve represents the Cascadia subduction zone.

2. Methodology

2.1. CMT Catalogue

All earthquake data was extracted from the Global Centroid Moment Tensor Catalog (Dziewonski et al.,1981). The catalogue is a database of global earthquakes recorded since 1976 with a minimum moment magnitude of 4.3. Constraints used in this research were: a date constraint from 1/1/1976 to 10/11/2018. No constraints were set on moment magnitude and earthquake depth.

2.2. Kostrov Summation

Kostrov (1974) showed that given the the sum of all moment tensors of a M_{ij} coherent deformation volume V with N number of earthquakes , the average strain ϵ_{ij} could be described as:

$$\epsilon_{ij} = \frac{1}{2\mu V} \sum_{n=1}^{N} M_{ij} \tag{1}$$

where μ is the shear modulus. The relationship above could be extended to describe the average strain rate $\frac{d\epsilon_{ij}}{dt}$:

$$\frac{d\epsilon_{ij}}{dt} = \frac{1}{2\mu V\tau} \sum_{n=1}^{N} M_{ij} \tag{2}$$

where τ is the time length of the earthquake catalogue record. A scalar strain rate can be calculated by substituting $_{ij}$ with the scalar moment tensor M_0. Brune (1968) showed that given the sum of scalar moment tensor M_0 we can express the plate velocity v by the following equation:

$$v = \frac{1}{\mu LW\tau} \sum_{n=1}^{N} M_0 \tag{3}$$

where L is the length of the fault on the surface and W is the displacement along the fault in its dip direction. The Kostrov summation makes the assumption that the deformation of each individual earthquake can be represented through the sum of moment tensors of all the earthquakes contained within a deforming volume V. The study region is then split into different areas of homogeneous deformation according to the type of focal mechanism and tectonic mechanism as shown in Figure 2.

2.3. Variable Calculation

A value of 3.3x10^{10}Nm^{-2} is used for μ to represent the rigidity of crustal rock (Stacey, 1992). The fault length L is determined using the Haversine formula that calculates the great-circle distance between two points on a sphere (Van Brummelen, 2013). The area A is calculated by employing a map projection technique to project longitude and latitude points on the map into a horizontal plane. The Albers Equal Conic Area Projection was chosen as the technique is most accurate with distances in mid-latitudes (Snyder, 1987). The seismogenic thickness d is calculated by using the average of all earthquake depths in each area. Subsequently, the volume V is calculated by:

$$V = Ad \tag{4}$$

τ is obtained by calculating the time difference between the earliest and most recent earthquake in the CMT catalogue of each distinct area. A Fortran programme, MTTK is used to obtain the dip δ of the fault plane. δ is chosen by evaluating its corresponding strike value to plate boundary and tectonic mechanism of the area. The fault displacement W is then calculated as:

$$W = \frac{d}{sin(\delta)} \tag{5}$$

2.4. Principal Strain Rates

For a double couple moment tensor, the smallest negative eigenvalue is equivalent to the strain rate on the P axis, the maximum compressional strain axis whereas the largest positive eigenvalue is equivalent to the strain rate of the T axis, the maximum extensional strain axis (Jost and Hermann, 1989). The MTTK program has an added functionality to decompose the summed up moment tensor of an area to its eigenvalues ξ and their corresponding dip δ and strike θ values. The strain rates along the principal axes direction can be calculated by substituting ξ into $Equation(2)$:

$$\frac{d\epsilon}{dt} = \frac{1}{2\mu V\tau}\xi cos(\delta) \tag{6}$$

where cos(δ) resolves the strain rate $\frac{d\epsilon}{dt}$ into its horizontal components. This conversion is necessary for data comparison with the tectonic mechanism as poles of rotation lie in the horizontal plane only (Jackson and McKenzie, 1988).

2.5. UNAVCO Geodetic Data

The UNAVCO plate motion calculator is used to obtain geodetic data in each area. 20 random points are generated within each area in which about 10 were selected. The points were then split into their respective sides along the plate boundary, using the plate on the other side as the reference frame as the assumption of the relative motion between plates producing the tectonic movement. An average across plate velocities in each area is calculated for data comparison. The MORVEL model (DeMets et al., 2010) is used as the data collected utilises four distinct observational methods to obtain local, unambiguous estimates of plate movement. Geodetic strain rates along the principal axis were calculated by using the UNAVCO Global Strain Rate Map (Kreemer et al. 2014). The data is reliable as the project inverts 22,415 number of geodetic velocities at 18,365 number of locations in which a great portion were studies around Western North America (Kreemer et al. 2014). An average of all strain rates bounded within each area was calculated.

Table 1. Comparison of plate velocity and principal axes strain rate values in the San Andreas Fault and Walker Lane region

Area	v/mmyr-1	UNAVCO v/mmyr-1	T-axis $\frac{d\epsilon}{dt}$/yr-1	UNAVCO T $\frac{d\epsilon}{dt}$/yr-1	P-axis $\frac{d\epsilon}{dt}$/yr-1	UNAVCO P $\frac{d\epsilon}{dt}$/yr-1
San Jacinto Fault	33.9	49.9	1.0e-07	1.2e-07	-1.0e-07	-1.0e-07
Los Angeles	2.0	48.7	2.5e-09	4.1e-08	-9.0e-09	-7.4e-08
Central C. Coast Ranges	2.7	51.2	1.5e-09	8.2e-08	-9.6e-09	-8.9e-08
South Walker Lane	0.7	50.3	2.7e-09	2.9e-08	-4.9e-10	-2.4e-08
San Francisco Bay Area	6.7	49.8	1.5e-08	9.1e-08	-2.5e-08	-9.7e-08
North Walker Lane	2.6	50.5	6.3e-09	3.3e-08	-3.4e-09	-2.1e-08

3. Results

3.1. San Andreas Fault and Walker Lane

The calculated plate velocities of the two seismic zones as shown in Table 1 have a mean value of 8.1mmyr^{-1} and a standard deviation of 12.8mmyr^{-1}. This is contrasted largely with the geodetic plate velocities with a mean value of 50.1mmyr^{-1} and a standard deviation of only 0.9 mmyr^{-1}. The calculated plate velocities have a much larger spread due to the San Jacinto Fault subregion in which its one order of magnitude bigger than the other values. Geodetic plate velocities are all larger than their respective calculated plate velocities. The San Jacinto Fault subregion has a percentage difference of 32.1%, the only subregion that is not above 85%. Average velocity difference in each area is shown in Figure 4 and the individual geodetic velocities of the whole San Andreas Fault and Walker Lane region is shown in Figure 5. The North American Plate moves at a 322° direction relative to the Pacific Plate at an average speed of 50.1mmyr^{-1}.

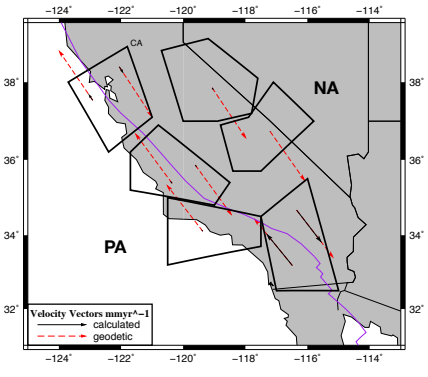

Figure 4. Velocity vectors of San Andreas Fault and Walker Lane Region.

The calculated T-axis strain rate and P-axis strain rate have very similar mean and standard deviation values: a mean of 2.2e-08yr^{-1} and -2.8e-08yr^{-1}, a standard deviation of 4.0e-08yr^{-1} and 3.8e-08yr^{-1} respectively. The geodetic T-axis strain rate and P-axis strain rate share this behaviour:

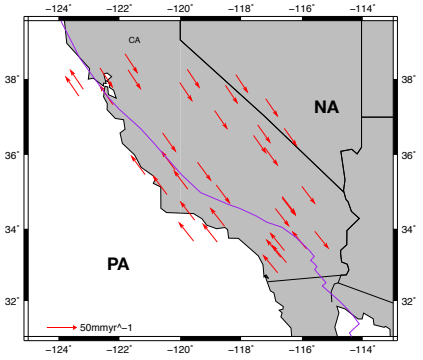

Figure 5. Individual geodetic velocities to show overall relative motion of Pacific and North American Plate.

mean of 6.6e-08yr^{-1} and -6.8e-08yr^{-1} respectively, a standard deviation of 3.7e-08yr^{-1} for both rates. However, the difference of mean values calculated strain rates and geodetic strain rates amount to a factor of about 3. This is prevalent in the percentage differences of T and P axis strain rates for all subregions except San Jacinto Fault are larger than 70%. San Jacinto Fault has a remarkably low percentage difference of 13.9% for T-axis strain rate and 4.3% for P-axis strain rate.

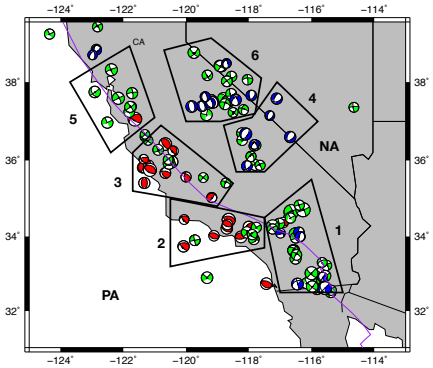

Figure 6. Boxed regions of coherent deformation within San Andreas fault and Walker Lane Region.

Most subregions in Figure 6 have a combination of two or more different types of seismicity, which lends to the difficulty of the summed-up focal mechanisms seen in Figure 7 to represent their respective areas.

Table 2. Comparison of plate velocity and principal axes strain rate values in the Gorda region

Area	v/mmyr-1	UNAVCO v/mmyr-1	T-axis $\frac{d\epsilon}{dt}$/yr-1	UNAVCO T $\frac{d\epsilon}{dt}$/yr-1	P-axis $\frac{d\epsilon}{dt}$/yr-1	UNAVCO P $\frac{d\epsilon}{dt}$/yr-1
Mendocino Fault	14.5	47.6	1.1e-07	2.7e-08	-1.1e-07	-4.5e-08
Gorda Intraplate	37.2	46.9	1.5e-07	1.5e-07	-1.5e-07	-7.9e-08
Gorda Ridge	0.5	47.1	3.5e-09	8.8e-08	-4.0e-10	-1.8e-08
East Blanco Fault	7.8	47.9	5.6e-08	3.8e-07	-5.3e-08	-1.9e-07
Cascadia Depression	2.0	48.8	3.9e-08	2.8e-07	-3.3e-09	-2.2e-07
West Blanco Fault	7.5	48.9	9.1e-08	1.3e-07	-7.2e-08	-4.7e-08

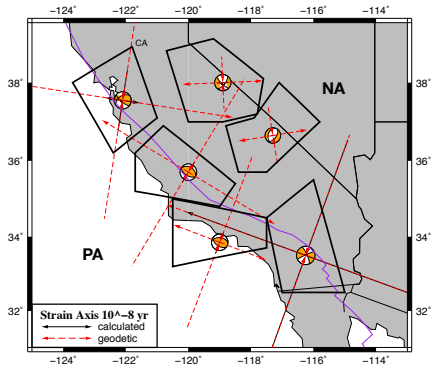

Figure 7. Summed-up focal mechanisms and principal-axes strain rate in San Andreas Fault and Walker Lane Region.

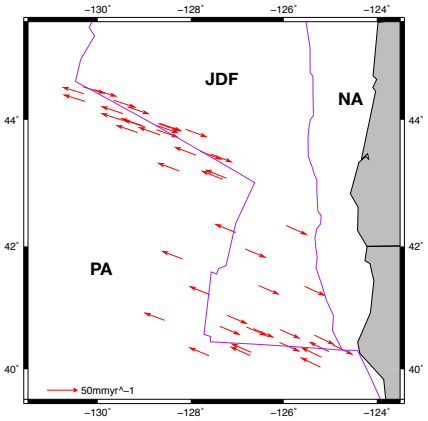

Figure 9. Individual geodetic velocities to show overall relative motion of Pacific and North American Plate.

The style of principal strain axes show that the compressive strain accumulation of the San Andreas Fault system has a NE-SW trend, while the Walker Lane Fault system has a near vertical NW-SE trend.

3.2. Gorda Region

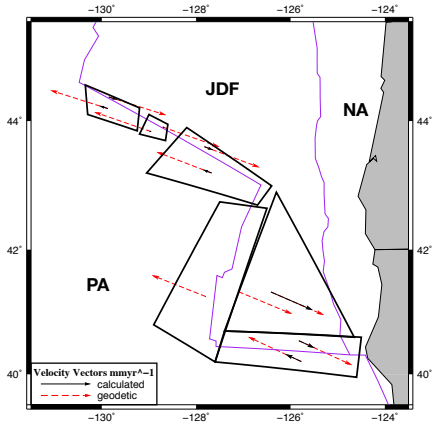

Figure 8. Velocity Vectors of Gorda region.

The standard deviation for calculated plate velocities in the Gorda region as shown in table 2 is relatively large at value of 13.5mmyr^{-1} relative to its mean 11.6mmyr^{-1} despite situated in the same tectonic regime. However, the geodetic plate velocities have a relatively small standard deviation of only 0.8mmyr^{-1} relative to a mean of 47.9mmyr^{-1}. The disparity in the two values between calculated and geodetic plate velocities can be seen through their percentage differences in Figure 8. All subregion exceed a percentage difference of 70% except the Mendocino Fault (69.5%) and the Gorda Intraplate (20.7%). The overall plate motion can be seen in Figure 9 with the Pacific Plate moving at a 289° direction relative the Juan De Fuca Plate at a speed of 47.9mmyr^{-1}.

The calculated principal axes strain rates have similar values for standard deviation and mean: a 5.4e-08yr^{-1} standard deviation and a 7.6e-08yr^{-1} mean for T strain rates; a 6.0e-08yr^{-1} standard deviation and a -6.6e-08yr^{-1} for P strain rates. Both T and P axes strain rates have a relatively large standard deviation with respect to their mean, to about a factor of 1. This contrast starkly with the geodetic principal axes strain rates with a mean of 1.75e-07yr^{-1} and -1.01e-07yr^{-1} for T-axis and P-axis respectively in which both are one order magnitude larger than their subsequent calculated partners. Figure 11 accentuates this difference in magnitude. There are however two exceptions to this (T, P): the Mendocino Fault(-321.3%,-146.8%) and the Gorda Intraplate(-1.7%,-93.7%) which the calculated strain axes are larger than the geodetic values. West Blanco Fault also exhibits this

Table 3. Comparison of plate velocity and principal axes strain rate values in the Explorer region

Area	v/mmyr-1	UNAVCO v/mmyr-1	T-axis $\frac{d\epsilon}{dt}$/yr-1	UNAVCO T $\frac{d\epsilon}{dt}$/yr-1	P-axis $\frac{d\epsilon}{dt}$/yr-1	UNAVCO P $\frac{d\epsilon}{dt}$/yr-1
Juan De Fuca Ridge	0.5	50.3	3.7e-09	8.4e-07	-3.7e-09	-4.7e-08
Sovanco Fault	10.2	52.2	8.2e-08	2.5e-07	-7.5e-08	-1.6e-07
Nootka Fault	3.5	52.8	4.1e-08	2.7e-07	-3.5e-08	-1.4e-07
Vancouver Islands	13.4	42.8	9.6e-08	1.1e-07	-9.0e-08	-2.2e-07
Explorer Ridge	2.6	47.8	2.8e-08	2.2e-07	-2.5e-08	-1.2e-07
Revere-Dellwood Fault	6.9	53.2	6.5e-08	1.6e-07	-6.4e-08	-1.3e-07
Winona Basin	23.9	54.0	4.4e-07	3.0e-07	-4.0e-07	-2.5e-07
Queen Charlotte Normal	2.9	50.1	3.7e-08	2.3e-08	-4.7e-09	-3.5e-08
Queen Charlotte Thrust	630.0	50.8	2.6e-06	7.5e-08	-7.1e-06	-3.3e-07

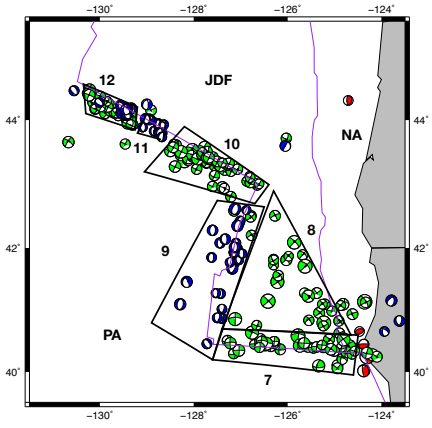

Figure 10. Boxed regions of coherent deformation within Gorda Region.

behaviour only on the P-axis strain rate (-52.9%). The remaining subregions have a percentage difference exceeding 70% on both principal axes.

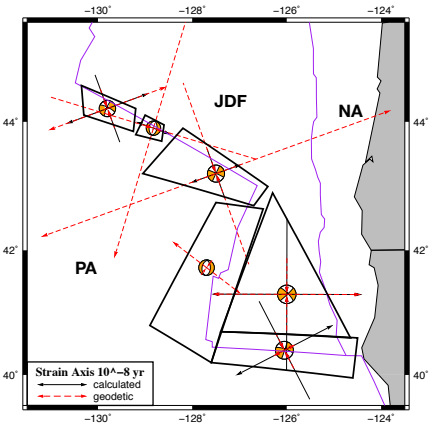

Figure 11. Summed-up focal mechanisms and principal-axes strain rate in Gorda region.

The seismicity of each subregion is made up of mostly one type of focal mechanism which is well represented in the summed up focal mechanism in Figure 11. The style of principal axes strain rates show a compressive strain accumulation trending NW-SE throughout the entire region except for the Gorda Intraplate and Cascadia Depression in which the latter is trending 20°.

3.3. Explorer Region

The Explorer region has the largest spread of calculated velocities so far, with a standard deviation of 207.5mmyr^{-1} and a mean of 77.1mmyr^{-1}. This is due to the Queen Charlotte fault thrust region that has a calculated velocity of 3 magnitudes larger than the smallest calculated velocity. Removing this region gives a standard deviation of 7.75mmyr^{-1} and a mean of 8.0mmyr^{-1}. However, this alteration fails to improve the likeliness of the dataset with the geodetic one, comprising of a standard deviation of 3.4mmyr^{-1} and a mean of 50.4mmyr^{-1}. The percentage difference between each area therefore is mostly poor as shown in Figure 12, with only two subregions lower than 70%: the Vancouver Islands (68.7%) and Winona Basin (55.7%). It is also important to note that the larger standard deviation in the geodetic velocities compared to the other two regions implies that the region is mostly not under the same tectonic regime. This is obvious when taken to account the presence of three different lithospheric plates as seen in Figure 13. We then have to break it up into subregions to study the region's plate motion. The Nootka Fault and the Vancouver Island sub-regions indicates the plate motion of the Juan De Fuca Plate relative to the North American Plate at a speed of 47.8mmyr^{-1} at an average 48.2° direction. The Queen Charlotte Fault and the Winona basin subregions show the plate motion of the Pacific Plate relative to the North American Plate of 51.6mmyr^{-1} at a 339.7° direction. The remaining subregion presents the plate motion of the Pacific Plate relative to the Juan De Fuca Plate of 50.9mmyr^{-1} at a 286.2° direction.

The calculated principal axes strain rates for both T and P axis has by far the largest spread compared to the other regions. The calculated T axis strain rate has a standard deviation of 1.41e-07yr^{-1} and a mean of 9.9e-08yr^{-1}; the calculated P axis strain rate has a standard deviation of 2.34e-06yr^{-1} and a mean of -8.67e-07yr^{-1}. Both principal

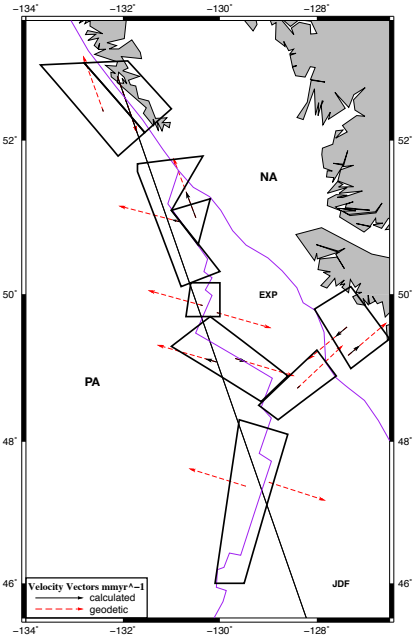

Figure 12. Velocity Vectors of Explorer region.

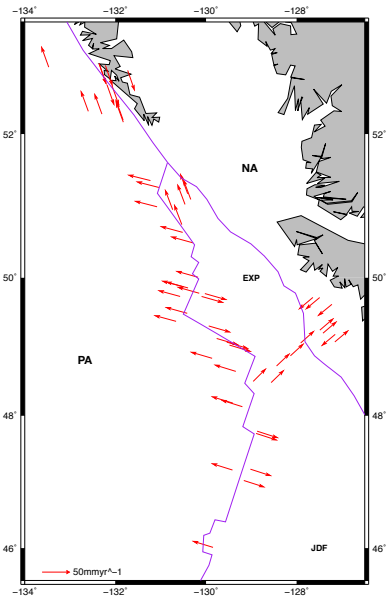

Figure 13. Individual geodetic velocities to show overall relative motion of all three plates within Explorer region.

axes strain rates have standard deviations that are a magnitude larger than their respective means. In contrast, geodetic strain rates have a standard deviation of 2.41e-07yr^{-1} relative to the mean of 2.49e-07^{-1} for T axis strain rates and a standard deviation of 9.5e-08yr^{-1} relative to the mean of -1.59e-07yr^{-1} for P axis strain rates. The standard deviation differs to their respective mean at most by a factor of about 1. The percentage difference varies the most in this region, from a percentage difference of 10.8% for T-axis strain rate in the Vancouver Islands to a whopping -3360.4% for T-axis strain rate in the Queen Charlotte Thrust as seen in Figure 15.

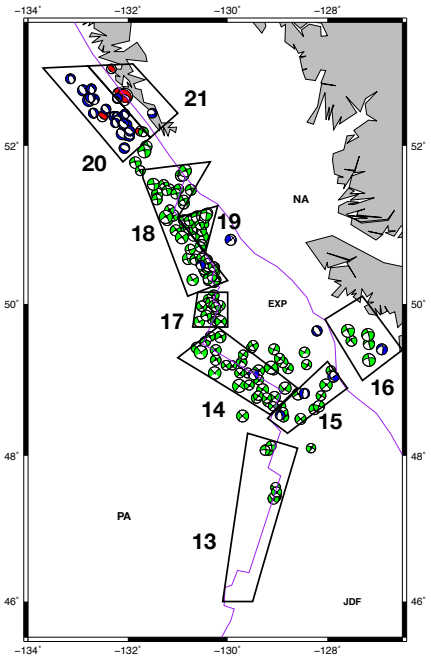

Figure 14. Boxed regions of coherent deformation within Explorer Region.

The relatively large standard deviation of the geodetic strain rates is due to the inhomogeneous tectonism of the area being studied as it involves three different lithospheric plates. Like the geodetic velocities, the strain rates have to be broken up into subregions of coherent deformation to study plate tectonism. The seismicity is largely homogenous at each subregion except for the Queen Charlotte Fault zone as seen in Figure 14. The southend of the Explorer region seem to have a near vertical compressive strain accumulation tending towards the NE-SW direction. The northend of the Explorer region and the other plates have compressive strain accumulation of about 26.3° direction. The Queen Charlotte Fault has two separate strain mechanisms acting on it, the Queen Charlotte Thrust aligned with the northend of Explorer region 's compressive strain accumulation, whereas the Queen Charlotte Normal is tending towards the NW-SE

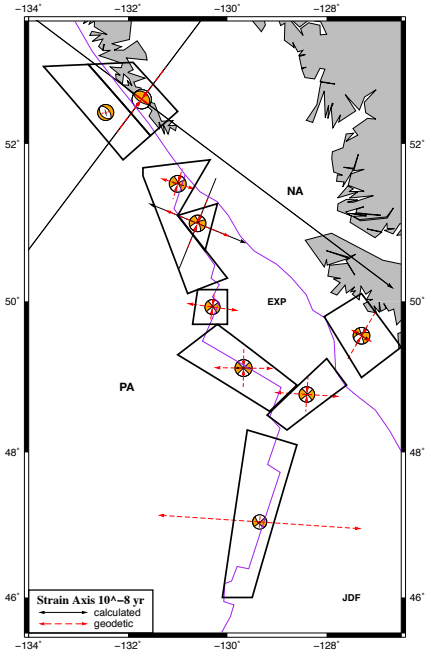

Figure 15. Summed-up focal mechanisms and principal-axes strain rate in Explorer region.

direction.

4. Discussion

4.1. Slow Earthquakes and Aseismic slip

4.1.1. Cascadia Subduction Zone

The Cascadia Subduction Zone between the Juan De Fuca Plate and the North American Plate remains unusually silent as seen in Figure 1. As subduction zones are known to generate the largest magnitude earthquakes, it would have been significant in studying the deformation of this tectonic regime. However, other papers have noted that unconventional earthquakes do indeed occur in this subduction zone. These slow earthquakes are low frequency earthquakes that release energy discontinuously over a period of hours to months compared to the seconds to minutes periodicity of regular earthquakes. These are predominately observed at the plate interface down-dip of the seismogenic zone (Hyndman et al, 1997). On the southern section they occur at depths of 25-47km (Plourde et al, 2015) while a 25-37km depth at the northern section nearer to the Vancouver islands (Bostock et al, 2012).

Detection of slow earthquakes is tricky due to lacking a distinct, impulsive body wave signature (Shelly et al, 2006). It requires specific techniques such as waveform stacking with the template of a low frequency earthquake. In other words, specific methods and parameters must be prepared in order to seek these elusive earthquakes. The CMT catalogue employs detection methods that are not able to identify slow earthquakes. The detection method used can only identify long period body waves of about 45s (Ekstrom et al, 2012). Even if slow earthquakes were detected, the algorithm used to calculate the moment tensor of the earthquake will be inaccurate because the duration of these earthquakes far exceeds the period of body wave (Ekstrom et al, 2012). Therefore, in order to incorporate these types of earthquakes, a new or modified algorithm of earthquake moment tensors must be used to study its relationship with the corresponding tectonic mechanisms.

4.1.2. Central San Andreas Fault System

The central region of the San Andreas Fault system is a relatively quiet zone compared to the northern and southern section of the system as seen in Figure 6. Many studies have pointed to the evidence of aseismic creep, similar to slow earthquakes where strain energy is released over a long period of time resulting in displacement without generation of earthquakes. This aseismic creep action along the Central San Andreas Fault System accommodates 36 ± 1 mmyr^{-1} of right lateral motion (Meade, 2005). This is important as 75% of North America-Pacific Plate motion is accounted for in the San Andreas Fault system whereas the remaining resides in the Walker Lane Fault system (Wallace, 1991). The Central California Coast Ranges is the only subregion within the Central San Andreas Fault system. Therefore, the percentage ratio of 70.3% between the aforementioned aseismic creep slip rate and the geodetic velocity in that subregion is used to represent the general uncertainty of aseismic slip in the California region. This result is not surprising due to the percentage difference between the calculated and geodetic plate velocities of the subregion being 94.7%.

4.2. Historical Earthquakes

The Global Centroid Moment Tensor Catalogue only detects earthquakes over the period from 1976 to the present day. This means we only have an earthquake dataset that indicates short-term deformation, which we used to calculate for long-term seismicity. The uncertainty from a relatively short earthquake catalogue is large considering the traditional earthquake cycle being about a few hundred years long. Simple probability indiciates most fault systems would have produced earthquakes and released strain energy in a time before 1976, and they therefore reside witin the interseismic stages at present. A study in New Zealand has shown representing long-term tectonism through short-term deformation with reasonable accuracy (Walcott, 1984). Noting several historical earthquakes such as the 1949 Puget sound earthquake and the 1906 San Francisco earthquake would have important implications of the tectonic regime of

their respective area today. Calculated velocity values with the added scalar moment of the 1906 San Francisco earthquake on the San Francisco Bay area is about 80.3mmyr^{-1}. This gives a percentage difference of -61.2% compared to the previously calculated 86.5% in the San Francisco Bay Area without considering the change in area of propagation. The 1857 Fort Tejon earthquake was also used to calculate the plate velocity of the Central California Coast Ranges region coming up to a value of 38.2mmyr^{-1}. This leads to a percentage difference of 25.4% in contrast to 94.7% from previously calculated values. The strain rates were not possible to calculate with magnitude values alone. These results show that historical earthquakes have a significant role in telling the story of tectonic evolution and therefore is a significant portion of the overall uncertainty.

4.3. Catalogue Uncertainty

The catalogue also has a constraint of detecting only earthquakes exceeding a certain magnitude. A minimum magnitude of 4.3 was found in the catalogue, therefore this is the upper limit for possible magnitude values of constraint. The catalogue also has a poor accuracy detecting earthquakes of $M < 5$ (Ekstrom et al, 2012). We used the International Seismological Centre event catalogue to incorporate 362 small earthquakes of the Juan De Fuca ridge and calculate for the resulting plate velocity with a value of 0.48mmyr^{-1}. Comparing this value to the calculated 0.46mmyr^{-1}, the percentage difference is only 4.3%. However, catalogue incompleteness of the ISC catalogue is also a subject of uncertainty. The strain rate could not be calculated due to the ISC catalogue not containing values for the six independent elements of a zeroth-order moment-tensor that represents the earthquake.

4.4. b-value

Region	b-value (LSRM)	b-value (MLM)
California	0.8235	0.5734
Gorda	0.8239	0.5516
Explorer	0.9157	0.6212
Overall	0.8736	0.5231

Table 4. b-value comparison of LSRM and MLM methods on the three regions and the overall study region

Catalogue completeness can be further quantified through an evaluation of the b-value. The Gutenberg-Richter law (Crampin, 2015) provides a power law relationship between the magnitude and frequency of earthquakes in a region:

$$log_{10}N = a - bM \tag{7}$$

where N is the number of earthquakes greater or equal to magnitude M, a is the decimal logarithm of the total number of earthquakes and the b-value is a measure of the number of small versus large earthquakes. The b-value is expected to lie within 0.8 to 1.2 for seismically active regions (Shearer, 2009). M_w is used to calculate for M in equation (7). The b and a-value are calculated through the least square regression method in which is sensitive to the occurrence of largest events (Amittrano, 2012). The a-value is ignored as it has insignificant seismic relevance. The maximum likelihood method (Aki, 1965) is also used to calculate b-value as expressed as:

$$b = \frac{log(e)}{M_{mean} - M_{min}} \tag{8}$$

where M_{mean} is the mean magnitude of earthquakes in the catalogue and M_{min} is the minimum magnitude of earthquakes in the catalogue. The maximum likelihood method negates the sensitivity issue as it provides an estimate controlled by the smallest, most numerous earthquakes (Amittrano, 2012).

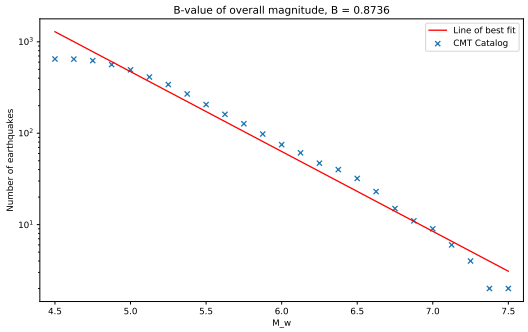

Figure 16. GR plot of overall study region

The b-values calculated by LSRM of the overall study region are within the expected 0.8 - 1.2 range. However, MLM calculated b-values all have values below 0.6, an indicator of under-representation of small earthquakes or an over-representation of large earthquakes (or both). This can be clearly seen in Figure 16 showing a deficit of small earthquakes M < 5.0. Large magnitude earthquakes > 7.0 are also under-represented. The lower summed moment tensor value due to the absence of small and large earthquakes could be one of the reasons why most of the calculated plate velocity and

strain rates in the overall study region are lower by 70% than their respective geodetic values.

The LSRM plotted b-value in Figure 17 suggests that the California region follows a similar trend with the overall region. Therefore, the same reasoning could be said for the rel-

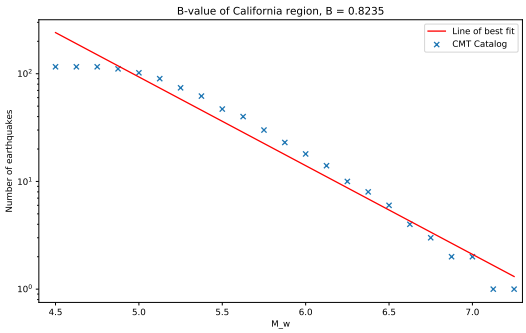

Figure 17. GR plot of California region

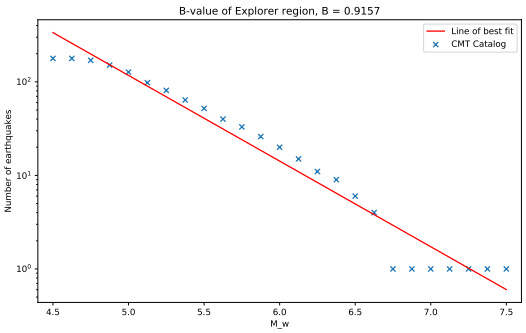

Figure 19. GR plot of Explorer region

atively low calculated velocities to geodetic values.

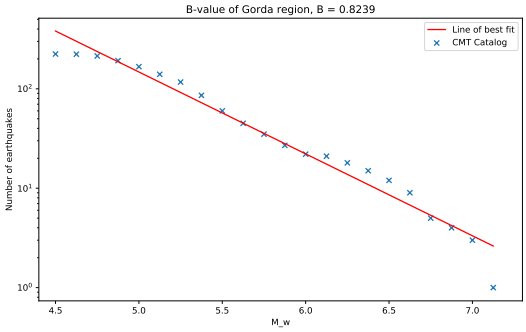

Figure 18. GR plot of Gorda region

The GR plot in Figure 18 indicates a similar trend in the Gorda region. However, $6.0 < M < 6.75$ shows an excess of larger earthquakes. This could explain why calculated velocity values in Mendocino fault and Gorda intraplate are one order magnitude larger than the other calculated velocities in the region. The larger calculated strain rates relative to their respective geodetic values for both Mendocino fault and Gorda intraplate could also be explained with this representation.

The plotted LSRM b-value in Figure 19 shows an excess of very large earthquakes $M > 7.25$. As calculated in the 1906 San Francisco earthquake and the 1857 Fort Tejon earthquake, earthquakes of $M > 7.0$ have a significant effect in the calculation of the total moment tensor summation. This could very well explain the unusually large calculated velocity and strain rates in the Queen Charlotte Normal relative to both its respective geodetic values and the other calculated velocity and strain rates in the region. The large calculated values of Winona basin can also be explained through this same reasoning.

4.5. Variable Analysis

4.5.1. Fault Length

The fault length in the plate velocity calculation is determined by best following the direction of the fault's strike. The strike is either referenced from the MTTK programme or followed by the fault trace on the map. The Haversine formula used to calculate two points of the fault length estimate is compared to values from the Google Earth Daft Logic Calculator. The percentage differences between the values were about 0.11% making the uncertainty in calculation irrelevant. The uncertainty for the straight line estimation on a fault trace that has notable curvature on the Great Circle path is also estimated. The method involves drawing two straight lines from the fault trace ends to encase the maximum curvature possible, as the fault trace cannot be longer than the encasing lines. This is done on the San Jacinto fault subregion as it has the most curved fault trace compared to other subregions. A percentage difference of -4.3% was calculated. Following up, a percentage difference of 4.1% between the calculated velocity and the velocity using the length of maximum curvature shows that it accounts for an insignificant uncertainty.

4.5.2. Area of Fault

Area of fault subregion is chosen to best resemble its coherent deformation. In some subregions such as the Queen Charlotte Fault zone, the seismicity in the area is less homogeneous and some uncertainty will be associated with the calculation. However, only 5 of the 21 subregions exhibit a notable degree of incoherent deformation using moment tensor summations in Figure 7,11,15 and therefore can be discounted. The uncertainty in the size of the box was also considered. The Juan De Fuca ridge subregion presents the largest amount of uncertainty due to having only 9 earthquakes for a largely unconstrained area. A percentage difference of -69.8% was found between calculated areas in

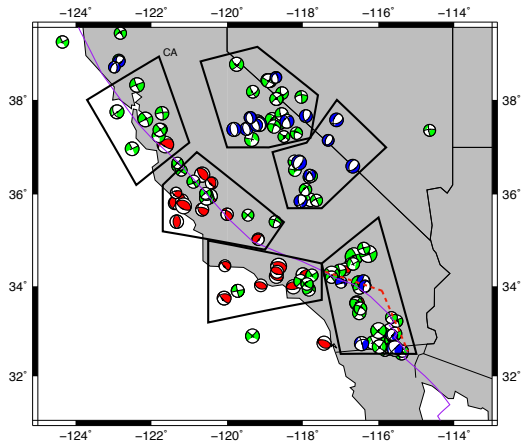

Figure 20. Red dashed lines represents maximum curvature possible for purple fault trace in the San Jacinto Fault sub region

Figure 21 and 41.1% for the subsequent velocity and strain rates. This uncertainty could only be applied locally to the Juan De Fuca ridge subregion as most subregions have earthquakes >20 that present well-constrained areas. The largest uncertainty in other subregions are about 10% and this leads to a 9.1% uncertainty in the calculated velocity and strain rate values.

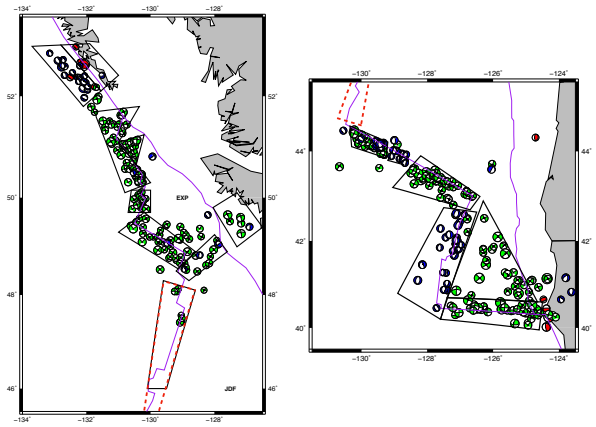

Figure 21. Red dashed lines represent box uncertainty of Juan De Fuca ridge sub region across the Explorer and Gorda region

4.5.3. Duration of Catalogue

The time period of the catalogue is calculated as the duration between the earliest and most recent earthquake events in a sub-region. There lies an uncertainty due to catalogue incompleteness that other (probably smaller) earthquakes were not registered in the catalogue, which could extend the time period. Using the time period from when the earthquake recordings in the CMT catalogue started to the present day (1976 - 2018), the percentage differences of only 6 time period values exceed 30%. The uncertainty becomes more prevalent for regions with fewer earthquakes such as the Juan De Fuca ridge (-275.5%) and Queen Charlotte Thrust (-237.4%). This could explain the unusually large velocities and strain rates of the Queen Charlotte Thrust and even the Winona Basin (-68.9%).

4.5.4. Seismogenic Thickness

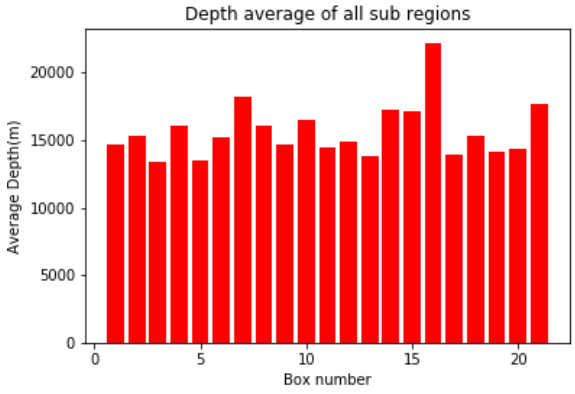

Figure 22. Average depth of all sub regions denoted by numbers

The depth average of earthquakes throughout the Western North America region all tend towards 15km, with the exception of Box 16 (Winona Basin) as seen in Figure 22. The conversation on the correct seismogenic thickness use in this study region especially within the Juan De Fuca plate has been pointed out in many studies. The 15 km depth average is deemed not appropriate as land adjacent stations used to record the oceanic earthquakes in the CMT catalogue have a low resolution of $\pm$ 3 km (Willoughby and Hyndman, 2005).

The depth of the oceanic plate throughout the region is not constant as it is colder the further away from spreading ridges, therefore the seismogenic thickness should increase with age (Burr and Solomon 1978). Ocean-bottom seismographs were used in one study to constraint earthquake depth with a range of 3 - 6 km depending on the subregion (Hyndman and Rogers, 1981). A depth of 3 km was usually used as an appropriate choice inferred from the probable depth of hydrothermal cooling of the crust near a spreading centre (Hyndman and Weichert, 1981). Another study of the Explorer region found an average depth of 10 km in the Explorer region with a standard deviation of 3 km (Braunmiller and Nabek, 2002). To evaluate the range of numbers from multiple papers, depths of 3 km, 6 km and 9

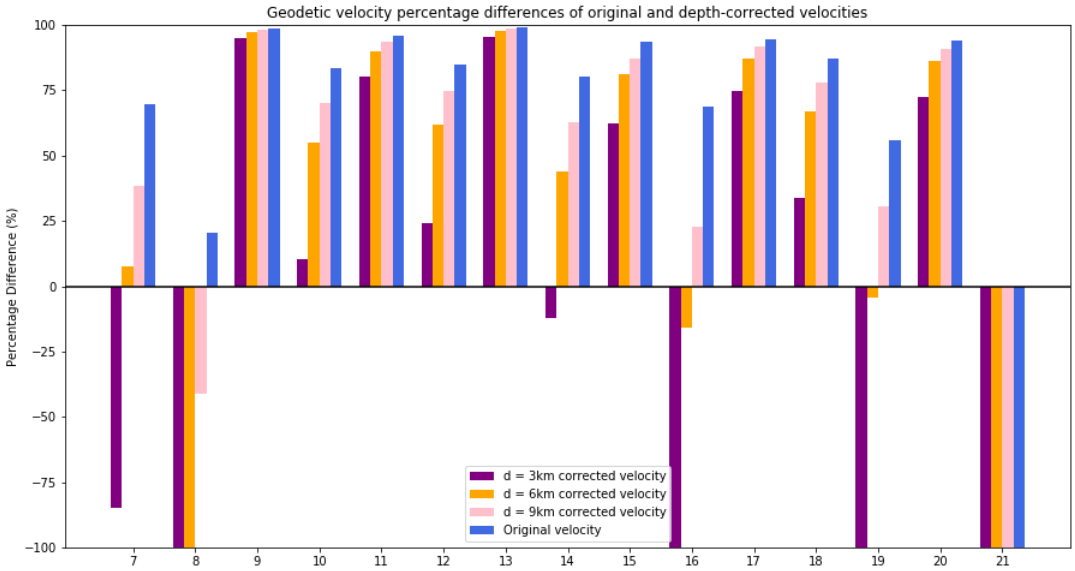

Figure 23. Geodetic velocities percentage differences for comparison of original and depth-corrected results

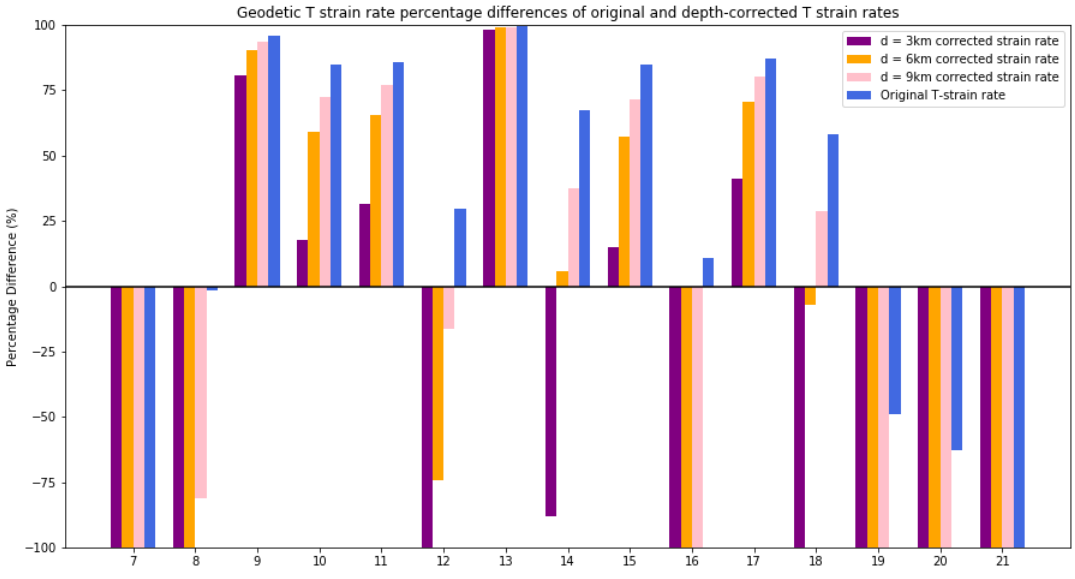

Figure 24. Geodetic T strain rates percentage differences for comparison of original and depth-corrected results

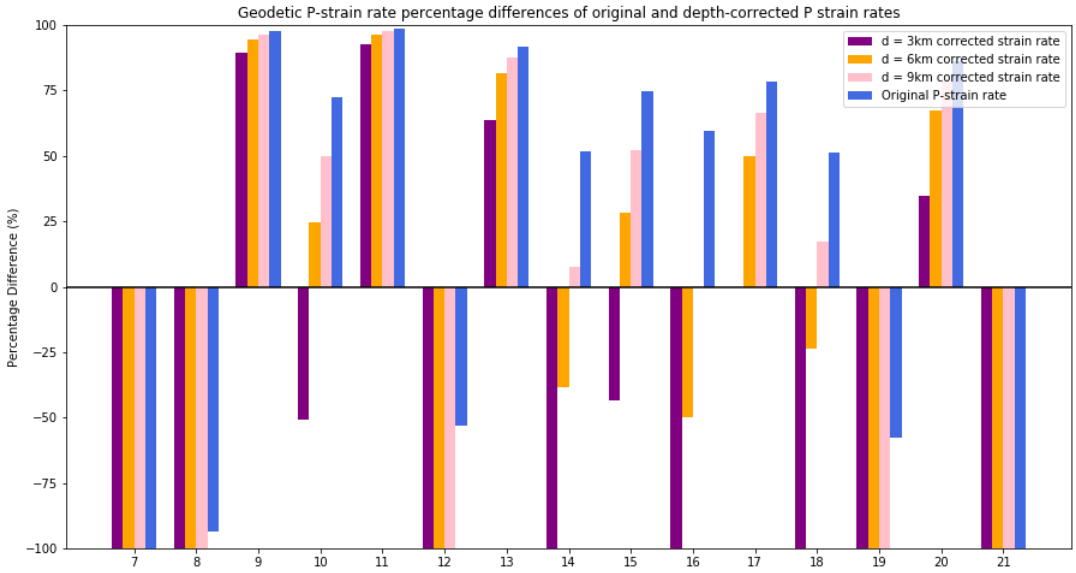

Figure 25. Geodetic P strain rates percentage differences for comparison of original and depth-corrected results

-km were used to recalculate plate velocity and strain rates. The percentage difference of the velocity and strain rates to their respective geodetic values for each depth correction are shown in Figure 23-25 for subregions of the Gorda and Explorer region.

The Gorda Ridge (9), Cascadia Depression (11), Juan De Fuca Ridge (13), Nootka Fault (15), Explorer Ridge (17) and the Queen Charlotte Normal (20) show a slight gradual decrease in velocity percentage difference with lower depth. The Gorda Ridge and the Juan De Fuca Ridge show the same behaviour on both the T and P strain axes. However,

notable strain rate percentage decrease in both axes are seen in the Nootka Fault (70.2%,31.5%) and Explorer Ridge (46.0%, 77.9%) with a 3 km depth correction (T axis %,P axis %). The highest accuracy of -0.4% percentage difference in the P strain rate with a 3 km depth correction is achieved at the Explorer ridge. The greatest percentage difference decrease with the corrected 3 km depth velocity calculation is in the South Blanco Fault (10), North Blanco Fault (12) and the Sovanco Fault (14) with a 73.3%, 60.6% and a 68.53% decrease respectively. The T strain rate percentage difference at the South Blanco Fault improves with a decrease of 67.3% at the 3 km depth, whereas the 6 km depth correction has the largest percentage decrease at the P strain rate relative to other depths. Both North Blanco fault and Sovanco Fault show a large increase in percentage difference for both strain axes. However, Sovanco fault shows a much higher accuracy at 5.9% percentage difference in the T strain rate with a 6 km depth correction and a 7.6% at the P strain rate with a 9 km depth correction.

The Mendocino (7) Fault and the Winona Basin (19) benefit most from the corrected 6 km depth velocity calculation with a decrease of 61.8% and 51.3% respectively. However, the percentage difference at this depth for both strain rates at the Mendocino Fault and Winona Basin are very large, exceeding 100%.

The Vancouver Islands (16) and the Revere Dellwood Fault (18) both showed a decrease of 53.0% through a 3 km depth correction and 6 km depth correction respectively. Both strain axes show poor accuracy at this depth.

The Gorda Intraplate (8) and the Queen Charlotte Thrust (21) are the only two subregions that showed the highest accuracy within their original depth velocity calculation. These two subregions have percentage differences that exceed to the thousands throughout both velocity and strain rates and therefore are not quantifiable.

Overall, a 3km depth correction improves the velocity percentage differences by large margins. It also generally shows the greatest improvement in accuracy relative to other depths. Strain rate percentage differences are hard to quantify as they are no real trend even between T and P axis on their respective subregions. However, depth corrections do lead to higher accuracy in strain rates despite no way to

identify the ideal depth in most subregions. This analysis suggests depth correction should be done for better accuracy of calculated data.

5. Conclusion

This study has shown that the Kostrov Summation leads to calculated velocity and strain rates with percentage differences on average more than 70% relative to the corresponding geodetic values from the UNAVCO calculator. The San Jacinto Fault showed the most accurate representation of its respective geodetic values, with a percentage difference of 32.1%, -1.7% and 4.3% for plate velocity, T-axis strain rate and P-axis strain rate respectively. The calculated velocities is more consistent in representing their corresponding geodetic values compared to calculated strain rates across all regions. A more thorough investigation on the eigenvalues provided by the MTTK programme could help better explain this.

The California region and Gorda region had more accurate results compared to the Explorer region, which may be due largely to the complexity of the tectonic regime. The California region is mainly affected by aseismic creep, absence of historical earthquakes and the under-representation of small earthquakes. Slow earthquakes, both the deficit of small earthquakes and the excess of large earthquakes, and the value chosen for seismogenic thickness play a significant role in the uncertainties involved in the Gorda region. Lastly, the Explorer region is influenced by the deficit of small earthquakes, excess of very large earthquakes and depth correction. Each variable involved in the calculation except seismogenic thickness show no notable uncertainties. However, the Juan De Fuca ridge is susceptible to these variable uncertainties as it is a poorly constrained area due to comprising of less than 10 earthquakes. Depth correction of 3 km improved results up to 0.4% for most subregions in the Gorda and Explorer region. This suggest the oceanic lithosphere that bounds most of the Gorda and Explorer region is about 3km. The Revere Dellwood Fault, the Mendocino Fault and the Winona Basin can be represented with a 6km depth represented by improved depth-corrected results.

The results indicate that short term seismicity can represent long term deformation to a reasonable accuracy, given the uncertainties listed are better constrained. The access to a more comprehensive catalogue, a historical earthquake record and geophysical surveys with tailored detection methods for slow earthquakes and aseismic slip will lead to a more accurate study.

6. Reference

Aki K. (1965), Maximum likelihood estimate of b in the formula log(n)=a - bm and its confidence limits. *Bulletin of the Seismological Society of America*, 43:237239.

Amitrano, D. (2012). Variability in the power-law distributions of rupture events. *The European Physical Journal Special Topics*, 205(1), pp.199-215.

Bostock, M., Royer, A., Hearn, E. and Peacock, S. (2012). Low frequency earthquakes below southern Vancouver Island. *Geochemistry, Geophysics, Geosystems*, 13(11), p.n/a-n/a.

Braunmiller, J. and Nblek, J. (2002). Seismotectonics of the Explorer region. *Journal of Geophysical Research*: Solid Earth, 107(B10), pp.ETG 1-1-ETG 1-25.

Brummelen, V. and Robert, G. (2013). *Heavenly mathematics: the forgotten art of spherical trigonometry*. Choice Reviews Online, 50(11), pp.50-6237-50-6237.

Brune, J. (1968). Seismic moment, seismicity, and rate of slip along major fault zones. *Journal of Geophysical Research*, 73(2), pp.777-784.

Burr, N. and Solomon, S. (1978). The relationship of source parameters of oceanic transform earthquakes to plate velocity and transform length. *Journal of Geophysical Research*, 83(B3), p.1193.

Crampin, S. and Gao, Y. (2015). The physics underlying Gutenberg-Richter in the earth and in the moon. *Journal of Earth Science*, 26(1), pp.134-139.

DeMets, C., Gordon, R. and Argus, D. (2010). Geologically current plate motions. *Geophysical Journal International*, 181(1), pp.1-80.

Dziewonski, A., Chou, T. and Woodhouse, J. (1981). Determination of earthquake source parameters from waveform data for studies of global and regional seismicity. *Journal of Geophysical Research*: Solid Earth, 86(B4), pp.2825-2852.

Ekstrm, G., Nettles, M. and Dziewoski, A. (2012). The global CMT project 20042010: Centroid-moment tensors for 13,017 earthquakes. *Physics of the Earth and Planetary*

Interiors, 200-201, pp.1-9.

Hyndman, R. and Rogers, G. (1981). Seismicity surveys with ocean bottom seismographs off western Canada. *Journal of Geophysical Research*, 86(B5), p.3867.

Hyndman, R. and Weichert, D. (1983). Seismicity and rates of relative motion on the plate boundaries of Western North America. *Geophysical Journal International*, 72(1), pp.59-82.

Hyndman, R., Yamano, M. and Oleskevich, D. (1997). The seismogenic zone of subduction thrust faults. The Island Arc, 6(3), pp.244-260.

Jackson, J. and McKenzie, D. (1988). The relationship between plate motions and seismic moment tensors, and the rates of active deformation in the Mediterranean and Middle East. *Geophysical Journal International*, 93(1), pp.45-73.

M. L. Jost and R. B. Herrmann (1989). A students guide to and review of moment tensors. *Seismological Research Letters*, 60(2):3757.

Kreemer, C., Blewitt, G. and Klein, E. (2014). A geodetic plate motion and Global Strain Rate Model. *Geochemistry, Geophysics, Geosystems*, 15(10), pp.3849-3889.

Meade, B. (2005). Block models of crustal motion in southern California constrained by GPS measurements. *Journal of Geophysical Research*, 110(B3).

Plourde, A., Bostock, M., Audet, P. and Thomas, A. (2015). Low-frequency earthquakes at the southern Cascadia margin. *Geophysical Research Letters*, 42(12), pp.4849-4855.

Shearer, P. (2009). *Introduction to seismology*. 2nd ed. Cambridge University Press.

Shelly, D., Beroza, G., Ide, S. and Nakamula, S. (2006). Low-frequency earthquakes in Shikoku, Japan, and their relationship to episodic tremor and slip. *Nature*, 442(7099), pp.188-191.

Snyder, J. (1987). *Map projections*. Washington, DC: U.S. Gov. Print. Off.

Stacey, F. and Lay, T. (1993). Physics of the Earth. *Physics Today*, 46(11), pp.88-89.

Walcott, R. (1984). The kinematics of the plate boundary zone through New Zealand: a comparison of short- and long-term deformations. *Geophysical Journal International*, 79(2), pp.613-633.

Wallace, R. (1991). *The San Andreas fault system, California*. Washington: United States Government Printing Office.

Willoughby, E. and Hyndman, R. (2005). Earthquake rate, slip rate, and the effective seismic thickness for oceanic transform faults of the Juan de Fuca plate system. *Geophysical Journal International*, 160(3), pp.855-868.

7. Appendix

Files	Functionality
main.py	a parser function used in almost every calculation involving subregion-by-subregion analysis. Utilises GMT format of psmeca denoting areas for easy copy and paste.
automate.py	a parser function for calculation of all subregions in a file
moment_summation.py	moment tensor summation calculation
variable_calculation.py	variables calculation
results_calculation.py	uses moment_summation.py and variable_calculation.py as inputs for calculation of velocity and strain rates
geodetic_calculation.py	uses UNAVCO data in text file to calculate for geodetic velocity and strain rates
b-value.py	calculates the b-value of a region and the overall study region
results_analysis.py	analysis of calculated vs geodetic values and uncertainties
main_map.gmt	draws entire study region, all seismicity and the borders of all subregions
Cal_region.gmt	zooms into only the California region with essentially all the features of main_map.gmt
vel_SA.gmt	plots average calculated and geodetic velocity on each other for comparison
vel_big_SA.gmt	plots all geodetic velocity to show overall relative plate movement
strain_SA.gmt	plots average calculated principal axes strain rates and geodetic strain rates on each other for comparison
README.txt	explains contents and methodology of codes in the TAR file

Table 5. Table of Content of electronic supplementary materials